Supporting Information *for*

Hybrid NiO-CuO mesoporous nanowires array with abundant oxygen vacancies and hollow structure for high-performance asymmetric supercapacitor

Zhenbin Fang[a], Sajid ur Rehman[a], Mingze Sun[a], Yupeng Yuan[a], Shaowei Jin[b], Hong Bi[a,*]

[a] *School of Chemistry and Chemical Engineering, Anhui University, Hefei 230601, P. R. China*

[b] *School of Physics and Materials Science, Anhui University, Hefei 230601, P. R. China*

* Corresponding author.

E–mail: bihong@ahu.edu.cn (H. Bi); Tel./Fax: +86 0551 63861279

Content

conducted under the same experimental conditions, respectively; (c) CV curves at different scan rates and (d) GCD curves at different current densities of Ni foam.

Fig. S13. The areal capacitances of the electrodes based on NiO-CuO with different molar ratios of Ni:Cu at different current densities.

Fig. S14. CV curves at different scan rates and GCD curves at different current densities of the electrodes based on NiO-CuO with different feed molar ratios of Ni:Cu: (a) and (b) 0:1; (c) and (d) 1:0; (e) and (f) 1:2, (g) and (h) 2:1.

Fig. S15. (a) Cycling performances of the electrodes based on NiO-CuO with different molar ratios of Ni:Cu at a current density of 20 mA cm^{-2}; SEM images of NiO-CuO with Ni:Cu (b) 1:0 and (c) 0:1 after 2 000 charge/discharge cycles.

Fig. S16. SEM image of the 3D porous graphene hydrogel (inset: the digital photo).

Fig. S17. (a) CV curves of PGH at different scan rates of 5, 10, 20, 30, 40 and 50 mV s^{-1}; (b) GCD curves of PGH at different current densities of 0.5, 1, 2, 3, 5 and 10 A g^{-1}, respectively.

Fig. S18. GCD curve of the NiO-CuO//PGH ASCs device within the first 10 charge/discharge cycles.

Fig. S19. XRD patterns of the NiO-CuO@Ni foam sample with Ni:Cu = 1:1 before and after 5 000 charge/discharge cycles.

Fig. S20. (a) Low and (b) high magnification SEM images of the NiO-CuO with Ni:Cu = 1:1 after 5 000 charge/discharge cycles.

Fig. S21. (a) TEM and (b) HR-TEM images of the NiO-CuO with Ni:Cu = 1:1 after 5 000 charge/discharge cycles.

Table S1. Previously reported data on metal oxides based electrodes in comparison with our work result.

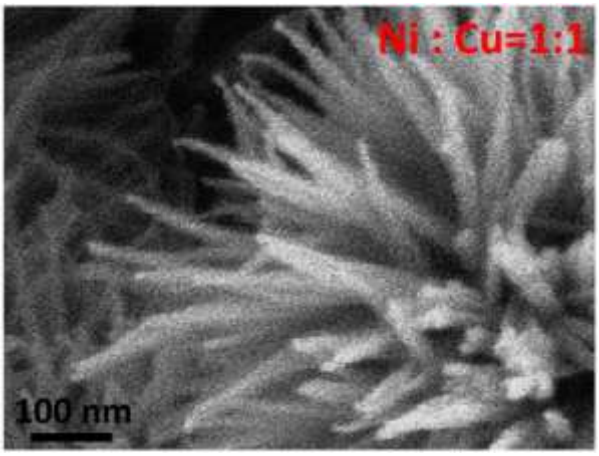

Fig. S1. SEM image of the NiO-CuO nanowires with Ni:Cu = 1:1.

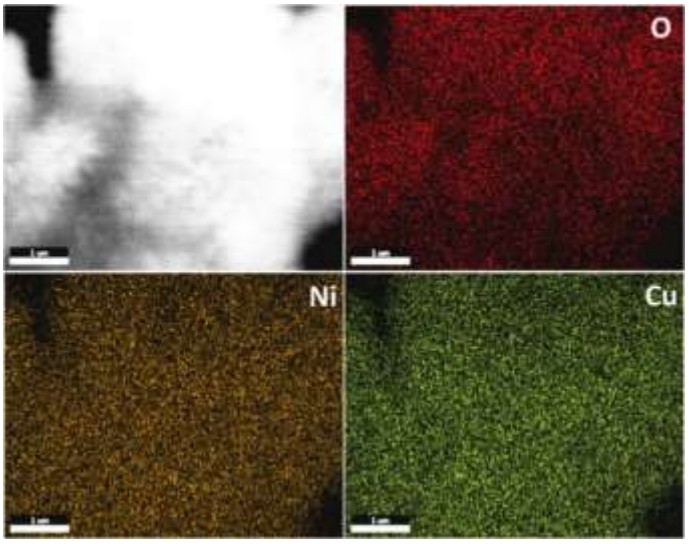

Fig. S2. The SEM image and the corresponding EDS color mappings of Ni, Cu and O elements in the sample of NiO-CuO with Ni:Cu = 1:1.

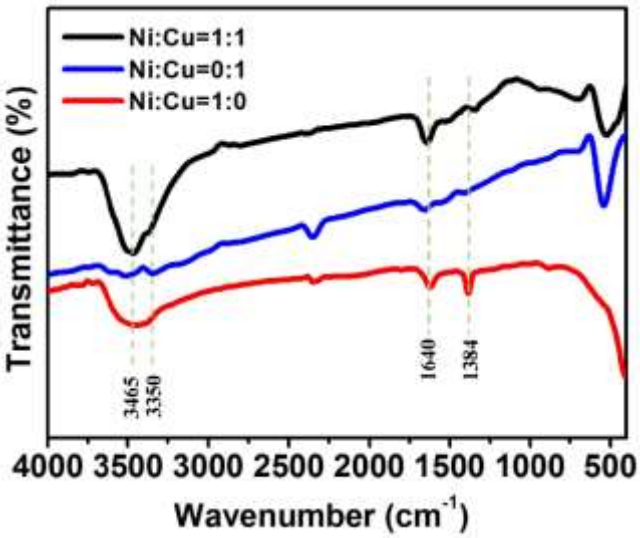

Fig. S3. The IR spectra of the NiO-CuO samples with Ni:Cu = 1:0, 0:1 and 1:1.

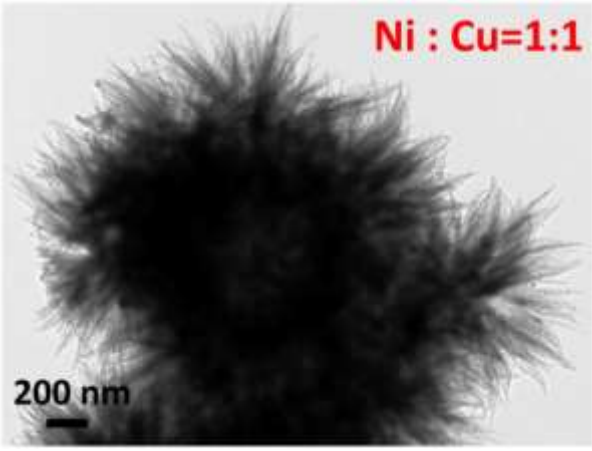

Fig. S4. TEM image of the hollow structure of NiO-CuO sample with Ni:Cu = 1:1.

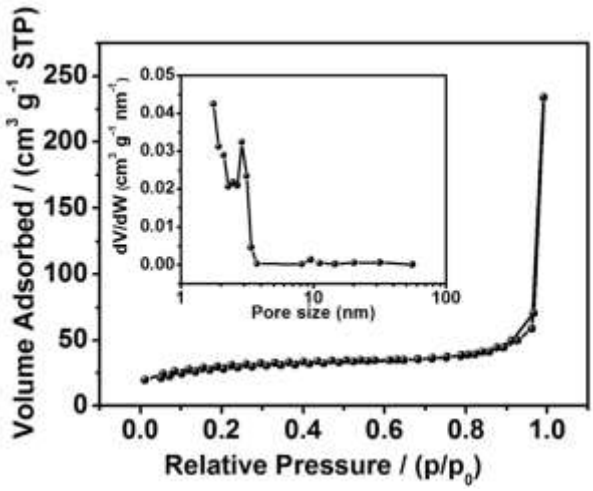

Fig. S5. Nitrogen adsorption−desorption isotherm of the NiO-CuO sample with Ni:Cu = 1:1 (inset: the pore-size distribution from the corresponding adsorption branch).

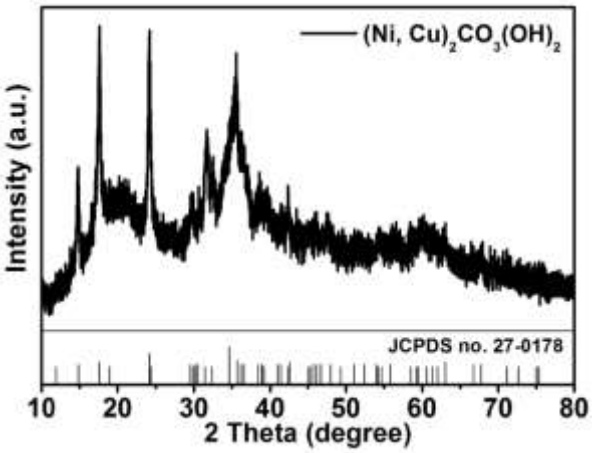

Fig. S6. XRD pattern of the hydrothermal product (Ni, Cu)$_2$CO$_3$(OH)$_2$ before annealing.

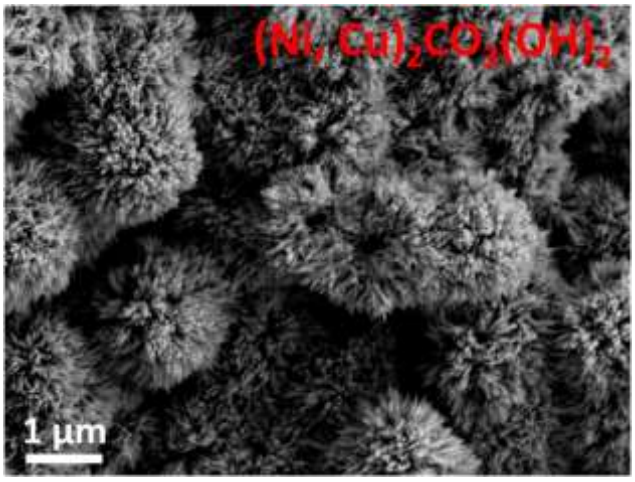

Fig. S7. SEM image of the hydrothermal product (Ni, Cu)$_2$CO$_3$(OH)$_2$ before annealing.

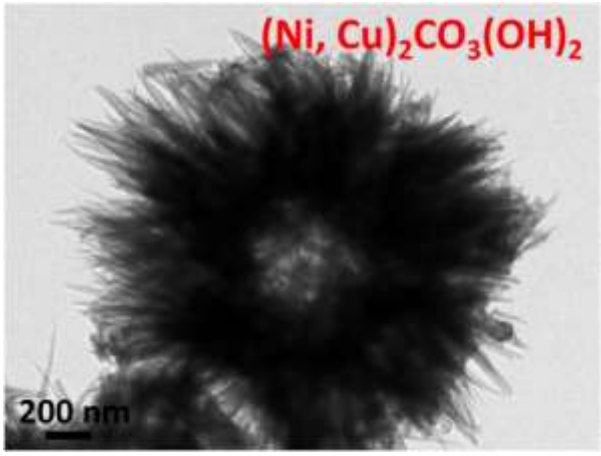

Fig. S8. TEM image of the hydrothermal product (Ni, Cu)$_2$CO$_3$(OH)$_2$ before annealing.

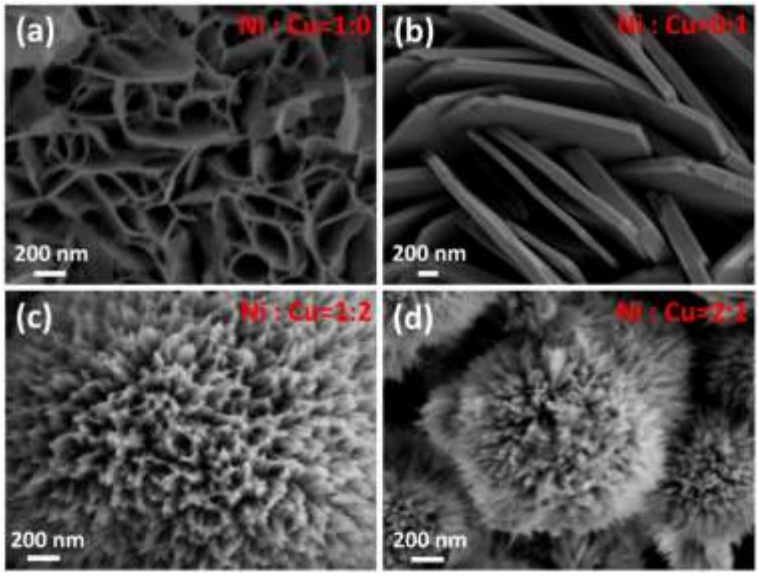

Fig. S9. High magnification SEM images of the NiO-CuO samples with different molar ratios of Ni:Cu = (a) 1:0, (b) 0:1, (c)1:2 and (d) 2:1.

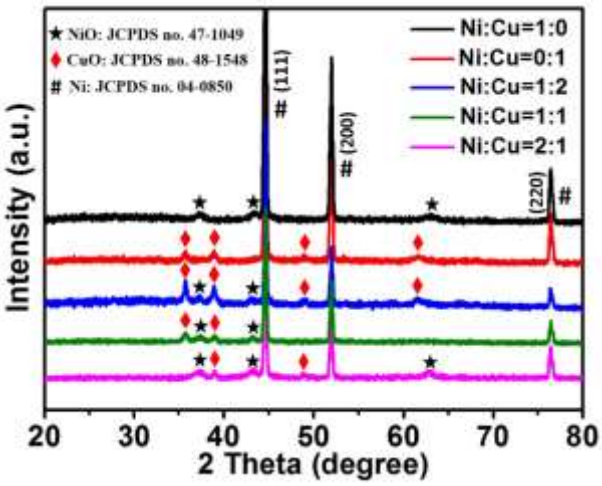

Fig. S10. XRD pattern of the NiO-CuO@Ni foam samples with different molar ratios of Ni:Cu = 1:0, 0:1, 1:2, 1:1 and 2:1.

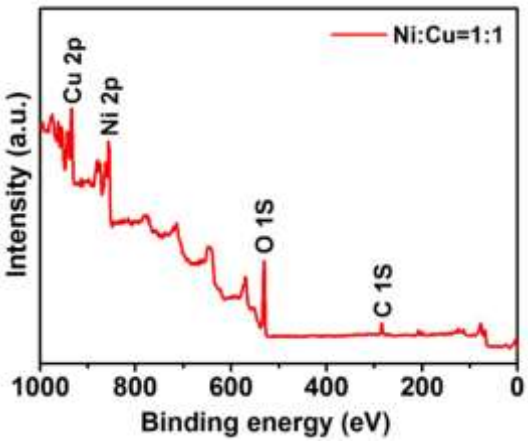

Fig. S11. The XPS survey spectrum of the NiO-CuO with Ni:Cu = 1:1.

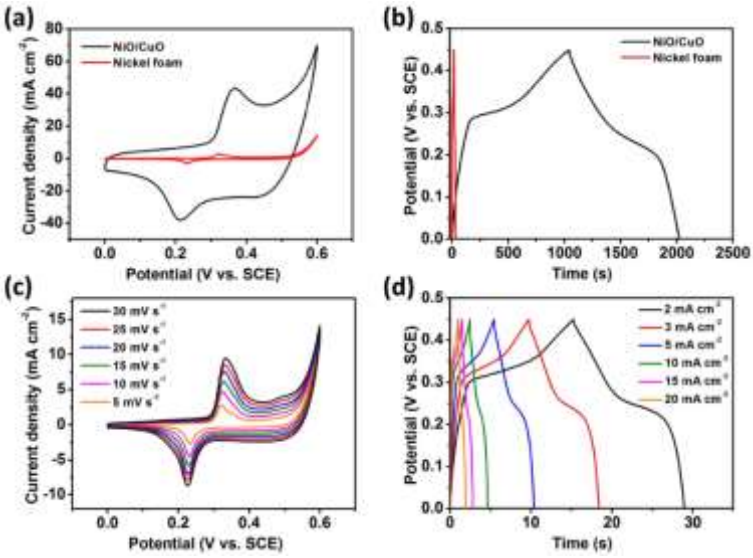

Fig. S12. (a) CV curves at a scan rate of 5 mV s^{-1} and (b) GCD curves at a current density of 2 mA cm^{-2} of the NiO-CuO with Ni:Cu = 1:1 and an individual Ni foam conducted under the same experimental conditions, respectively; (c) CVs at different scan rates and (d) GCDs at different current densities of Ni foam.

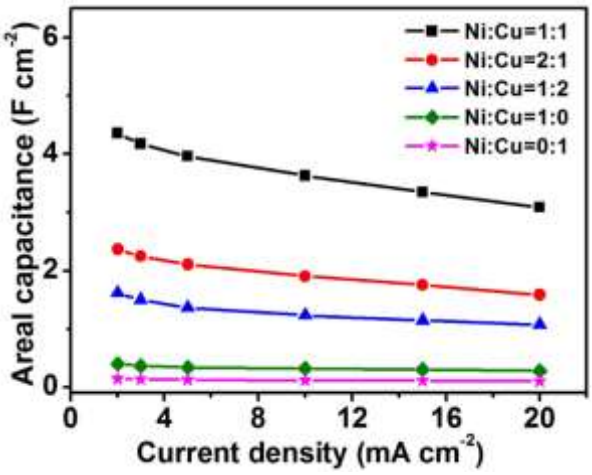

Fig. S13. The areal capacitances of the electrodes based on NiO-CuO with different molar ratios of Ni:Cu at different current densities.

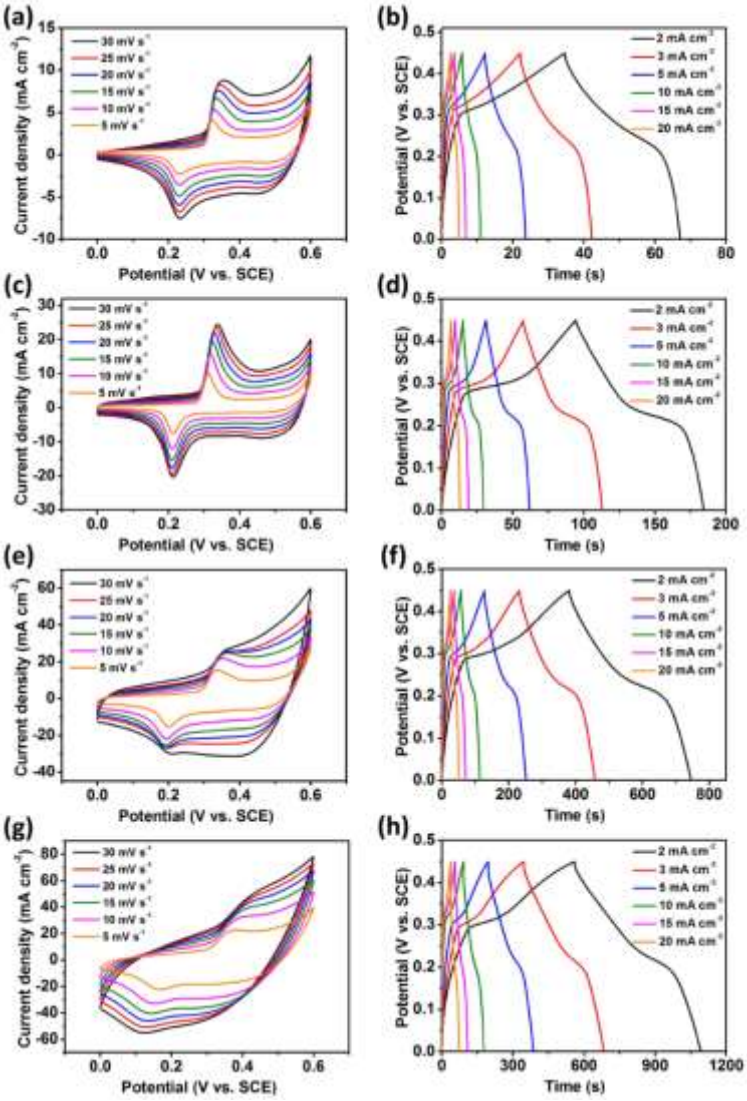

Fig. S14. CV curves at different scan rates and GCD curves at different current densities of the electrodes based on NiO-CuO with different feed molar ratios of Ni:Cu: (a) and (b) 0:1; (c) and (d) 1:0; (e) and (f) 1:2, (g) and (h) 2:1.

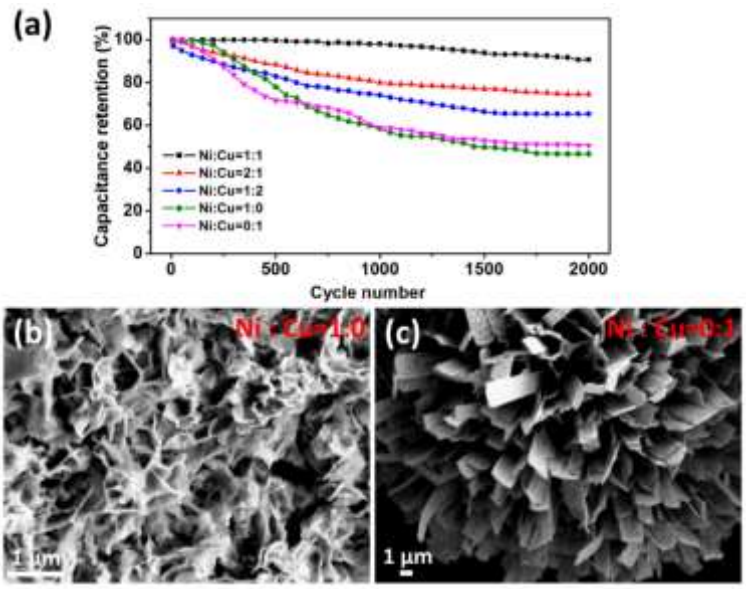

Fig. S15. (a) Cycling performances of the electrodes based on NiO-CuO with different molar ratios of Ni:Cu at a current density of 20 mA cm^{-2}; SEM images of NiO-CuO with Ni:Cu (b) 1:0 and (c) 0:1 after 2 000 charge/discharge cycles.

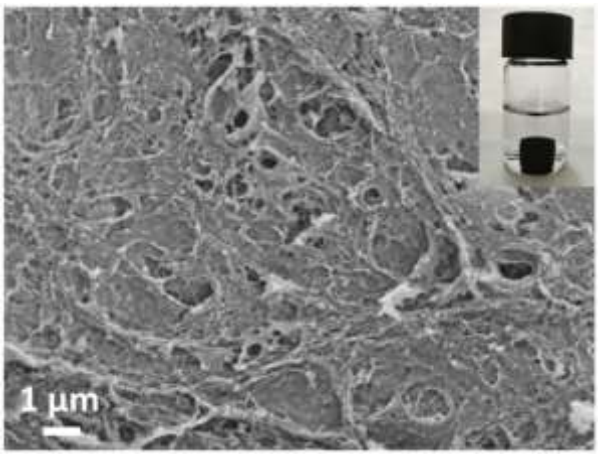

Fig. S16. SEM image of the 3D porous graphene hydrogel (inset: the digital photo).

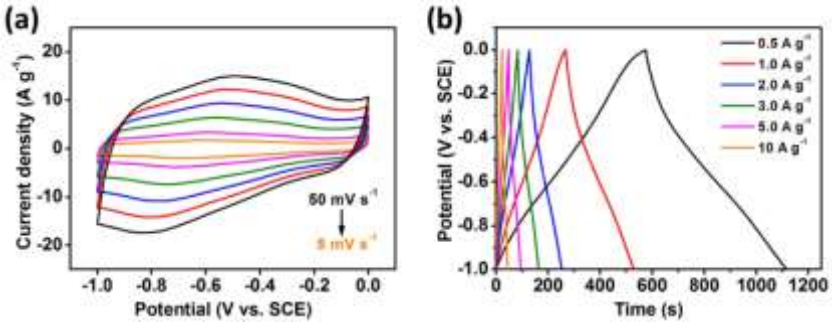

Fig. S17. (a) CV curves of PGH at different scan rates of 5, 10, 20, 30, 40 and 50 mV s^{-1}; (b) GCD curves of PGH at different current densities of 0.5, 1, 2, 3, 5 and 10 A g^{-1}, respectively.

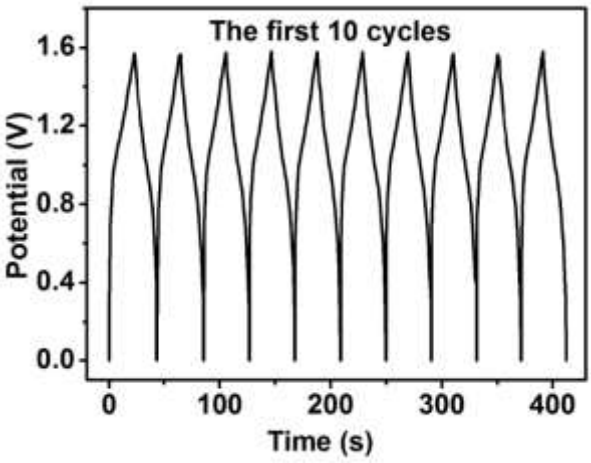

Fig. S18. GCD curve of the NiO-CuO//PGH ASCs device within the first 10 charge/discharge cycles.

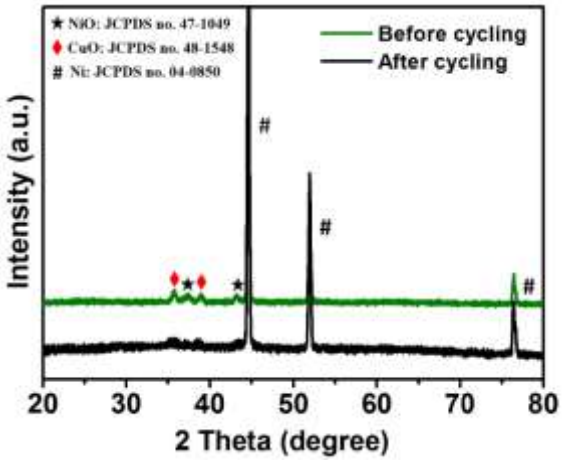

Fig. S19. XRD patterns of the NiO-CuO@Ni foam sample with Ni:Cu = 1:1 before and after 5 000 charge/discharge cycles.

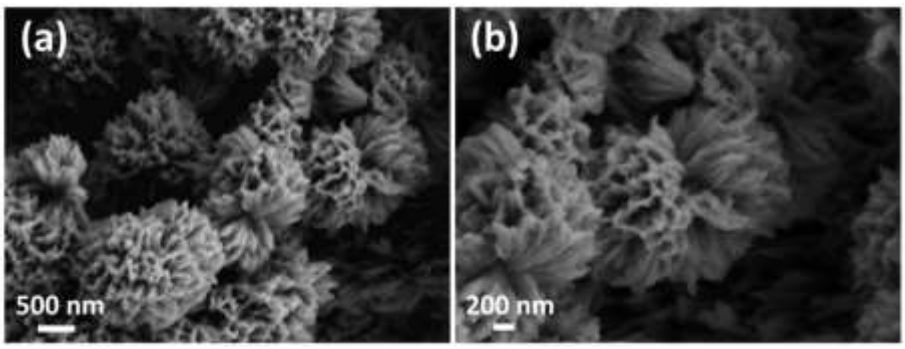

Fig. S20. (a) Low and (b) high magnification SEM images of NiO-CuO with Ni:Cu = 1:1 after 5 000 charge/discharge cycles.

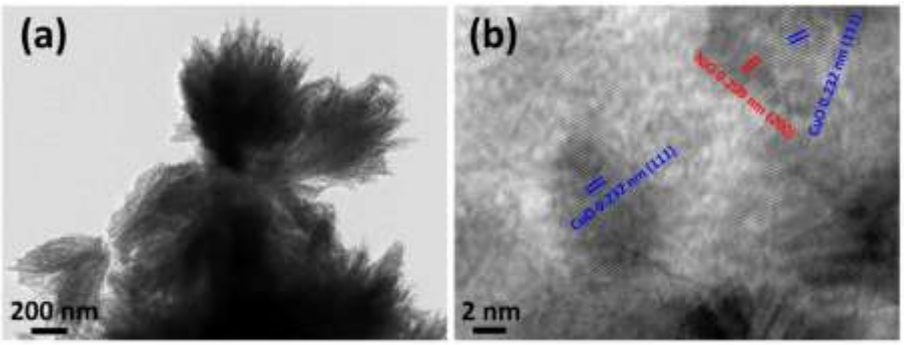

Fig. S21. (a) TEM and (b) HR-TEM images of the NiO-CuO with Ni:Cu = 1:1 after 5 000 charge/discharge cycles.

Table S1. Previously reported data on metal oxides based electrodes in comparison with our work result.

Materials	Specific capacitance ($F\ g^{-1}$)	Areal capacitance ($F\ cm^{-2}$)	Current density or scan rate	Electrolyte	Reference
NiO	302	-	1 $A\ g^{-1}$	6 M KOH	S1
CuO	431	1.51	3.5 mA cm^{-2}	3 M KOH	S2
Cu2O/CuO/Co_3O_4	318	-	0.5 $A\ g^{-1}$	3 M KOH	S3
NiO/NiMn-LDH	937	-	0.5 $A\ g^{-1}$	3 M KOH	S4
$CuCo_2O_4$/CuO	781	-	2 mV s-1	1 M KOH	S5
$Ni_{0.99}Cu_{0.01}O$	559	-	0.3 A g-1	6 M KOH	S6
Ni/NiO	526	-	1 $A\ g^{-1}$	3 M KOH	S7
NiO/α-$Ni(OH)_2$	707	-	2 $A\ g^{-1}$	2 M KOH	S8
Ni-Co binary hydroxide	1030	-	1 mg cm^{-2}	6 M KOH	S9
NiO@MnO_2	266.7	-	0.5 $A\ g^{-1}$	2 M KOH	S10
NiO-Co_3O_4	801	-	1 $A\ g^{-1}$	3 M KOH.	S11
ZnO-NiO	649	-	5.8 $A\ g^{-1}$	3 M KOH	S12
Cu/Ni-based manganese dioxide	374	-	0.25 $A\ g^{-1}$	1 M Na_2SO4	S13
$NiCo_2O_4$ nanowires	743	-	1 $A\ g^{-1}$	1 M KOH	S14
$NiCu(OH)_2CO_3$	971	-	1 $A\ g^{-1}$	6 M KOH	S15
NiO-CuO	1450.8	4.35	2 mA cm^{-2}	3 M KOH	Our work

References

[S1] X. Ren, C. Guo, L. Xu, T. Li, L. Hou and Y.Wei, *ACS Appl. Mater. Inter.*, 2015, 7, 19930-19940.

[S2] S. E. Moosavifard, M. F. El-Kady, M. S. Rahmanifar, R. B. Kaner and M. F. Mousavi, *ACS Appl. Mater. Inter.*, 2015, 7, 4851-4860.

[S3] M. Kuang, T. T. Li, H. Chen, S. M. Zhang, L. L. Zhang and Y. X. Zhang, *Nanotechnology*, 2015, 26, 304002.

[S4] P. F. Liu, J. J. Zhou, G. C. Li, M. K. Wu, K. Tao, F. Y. Yi, W. N. Zhao and L. Han *Dalton. Trans.*, 2017, 46, 7388-7391.

[S5] A. Shanmugavani and R. K. Selvan, *Electrochim. Acta*, 2016, 188, 852-862.

[S6] G. Yuan, Y. Liu, M. Yue, H. Li, E. Liu, Y. Huang and D. Kong, *Ceram. Int.*, 2014, 40, 9101-9105.

[S7] Y. Zhang, M. Park, H. Y. Kim and S. J. Park, *J. Colloid Interf. Sci.*, 2017, 500, 155-163.

[S8] B. K. Kim, V. Chabot and A. Yu, *Electrochim. Acta*, 2013, 109, 370-380.

[S9] X. Sun, G. Wang, H. Sun, F. Lu, M. Yu and J. Lian, *J. Power Sources*, 2013, 238, 150-156.

[S10] J. Chen, Y. Huang, C. Li, X. Chen and X. Zhang, *Appl. Surf. Sci.*, 2016, 360, 534-539.

[S11] X. W. Wang, D. L. Zheng, P. Z. Yang, X. E. Wang, Q. Q. Zhu, P. F. Ma and L. Y. Sun, *Chem. Phys. Lett.*, 2017, 667, 260-266.

[S12] H. Pang, Y. Ma, G. Li, J. Chen, J. Zhang, H. Zheng and W. Du, *Dalton. Trans.*, 2012, 41, 13284-13291.

[S13] H. Chen, X. Q. Qi, M. Kuang, F. Dong and Y. X. Zhang, *Electrochim. Acta*, 2016, 212, 671-677.

[S14] H. Jiang, J. Ma, and C. Li, *Chem. Commun.*, 2012, 48, 4465-4467.

[S15] X. Zheng, Y. Ye, Q.Yang, B. Geng and X. Zhang, *Chem. Eng. J.*, 2016, 290: 353-360.